



Contents lists available at ScienceDirect

## Journal of Integrative Medicine

journal homepage: [www.jcimjournal.com/jim](http://www.jcimjournal.com/jim)  
[www.journals.elsevier.com/journal-of-integrative-medicine](http://www.journals.elsevier.com/journal-of-integrative-medicine)



### Original Research Article

## Luteolin protects against myocardial ischemia/reperfusion injury by reducing oxidative stress and apoptosis through the p53 pathway



Pan Zhai <sup>a</sup>, Xiao-hu Ouyang <sup>a</sup>, Meng-ling Yang <sup>a</sup>, Lan Lin <sup>a</sup>, Jun-yi Li <sup>a</sup>, Yi-ming Li <sup>b</sup>, Xiang Cheng <sup>c,d</sup>, Rui Zhu <sup>a,\*</sup>, De-sheng Hu <sup>a,d,e,\*</sup>

<sup>a</sup> Department of Integrated Traditional Chinese and Western Medicine, Union Hospital, Tongji Medical College, Huazhong University of Science and Technology, Wuhan 430022, Hubei Province, China

<sup>b</sup> Department of Critical Care Medicine, Zhongnan Hospital of Wuhan University, Wuhan 430071, Hubei Province, China

<sup>c</sup> Department of Cardiology, Union Hospital, Tongji Medical College, Huazhong University of Science and Technology, Wuhan 430022, Hubei Province, China

<sup>d</sup> Hubei Key Laboratory of Biological Targeted Therapy, Union Hospital, Tongji Medical College, Huazhong University of Science and Technology, Wuhan 430022, Hubei Province, China

<sup>e</sup> China-Russia Medical Research Center for Stress Immunology, Union Hospital, Tongji Medical College, Huazhong University of Science and Technology, Wuhan 430022, Hubei Province, China

### ARTICLE INFO

#### Article history:

Received 1 September 2023

Accepted 13 August 2024

Available online 7 September 2024

#### Keywords:

P53 signaling pathway

Myocardial ischemia/reperfusion injury

Apoptosis

Oxidative stress

Luteolin

Network pharmacology

### ABSTRACT

**Objective:** Myocardial ischemia/reperfusion injury (MIRI) is an obstacle to the success of cardiac reperfusion therapy. This study explores whether luteolin can mitigate MIRI by regulating the p53 signaling pathway.

**Methods:** Model mice were subjected to a temporary surgical ligation of the left anterior descending coronary artery, and administered luteolin. The myocardial infarct size, myocardial enzyme levels, and cardiac function were measured. Latent targets and signaling pathways were screened using network pharmacology and molecular docking. Then, proteins related to the p53 signaling pathway, apoptosis and oxidative stress were measured. Hypoxia/reoxygenation (HR)-incubated HL1 cells were used to validate the effects of luteolin in vitro. In addition, a p53 agonist and an inhibitor were used to investigate the mechanism.

**Results:** Luteolin reduced the myocardial infarct size and myocardial enzymes, and restored cardiac function in MIRI mice. Network pharmacology identified p53 as a hub target. The bioinformatic analyses showed that luteolin had anti-apoptotic and anti-oxidative properties. Additionally, luteolin halted the activation of p53, and prevented both apoptosis and oxidative stress in myocardial tissue in vivo. Furthermore, luteolin inhibited cell apoptosis, JC-1 monomer formation, and reactive oxygen species elevation in HR-incubated HL1 cells in vitro. Finally, the p53 agonist NSC319726 downregulated the protective attributes of luteolin in the MIRI mouse model, and both luteolin and the p53 inhibitor pifithrin- $\alpha$  demonstrated a similar therapeutic effect in the MIRI mice.

**Conclusion:** Luteolin effectively treats MIRI and may ameliorate myocardial damage by regulating apoptosis and oxidative stress through its targeting of the p53 signaling pathway.

Please cite this article as: Zhai P, Ouyang XH, Yang ML, Lin L, Li JY, Li YM, Cheng X, Zhu R, Hu DS. Luteolin protects against myocardial ischemia/reperfusion injury by reducing oxidative stress and apoptosis through the p53 pathway. *J Integr Med.* 2024; 22(6): 652–664.

© 2024 Shanghai Yueyang Hospital Affiliated to Shanghai University of Traditional Chinese Medicine. All rights are reserved, including those for text and data mining, AI training, and similar technologies.

### 1. Introduction

Acute myocardial infarction is a prevalent cardiovascular condition characterized by significant morbidity and mortality on a global scale [1]. Revascularization therapy has become the standard treatment for patients with acute myocardial infarction [2], which

\* Corresponding authors at: Department of Integrated Traditional Chinese and Western Medicine, Union Hospital, Tongji Medical College, Huazhong University of Science and Technology, Wuhan 430022, Hubei Province, China.

E-mail addresses: zhur@hust.edu.cn (R. Zhu), desheng.hu@hust.edu.cn (D.S. Hu).

may however lead to myocardial ischemia/reperfusion injury (MIRI) [3,4]. The apoptosis of cardiomyocytes is an important mechanism of MIRI, which may impair myocardial function. However, drugs aimed at mitigating myocardial cell apoptosis and their potential mechanisms necessitate further study [5].

Luteolin, also known as 3',4',5,7-tetrahydroxy flavone, is primarily sourced from fruits, vegetables, and edible parts of various plants [6]. Luteolin has antioxidative, anticancer, antimicrobial, antidiabetic, anti-inflammatory, and neuroprotective properties, making it widely beneficial in the management of various ailments [7]. As an anticancer agent it has been shown to induce apoptosis and cell cycle arrest [6]. It can also inhibit nuclear factor-E2 like bZIP transcription factor 2 to promote the expression of heme oxygenase 1, thereby exerting significant protective effects during oxidative stress [8]. Currently, the attention to the luteolin's application in cardiovascular diseases is gradually gaining [9,10]. Previous studies have demonstrated that luteolin can reduce the mortality rate among individuals suffering from coronary heart disease, as well as ameliorate myocardial damage [11–14]. However, the underlying mechanism through which luteolin exerts its cardioprotective effect in MIRI is not yet known.

To investigate the mechanism by which luteolin exerts its cardioprotective effects, we performed *in vitro* and *in vivo* experiments to measure luteolin's suppressive effect on the phosphorylation of p53 and its ability to protect cardiomyocytes from ischemia/reperfusion injury. This research emphasizes the cardioprotective role of luteolin in mitigating myocardial injury through the inhibition of p53-mediated apoptosis and oxidative stress.

## 2. Materials and methods

### 2.1. Materials

Luteolin (purity > 98%; CAS: 491-70-3) and NSC319726 (purity > 95%; CAS: 71555-25-4) were purchased from Shanghai Aladdin Bio-Chem Technology Co., Ltd. (Shanghai, China). Pifithrin- $\alpha$  (purity > 98%, CAS: 60477-38-5) was purchased from Shanghai Macklin Biochemical Technology Co., Ltd. (Shanghai, China). Luteolin, NSC319726, and pifithrin- $\alpha$  were dissolved in dimethyl sulfoxide (DMSO) and subsequently mixed with phosphate buffered saline (PBS) to achieve a final solution with a DMSO concentration below 0.01%.

### 2.2. Animals

This study used 8 weeks old male C57BL/6 mice (Beijing Vital River Laboratory Animal Technology Co., Ltd., Beijing, China) that had been raised in a specific-pathogen-free environment with temperature at  $(24 \pm 2)^\circ\text{C}$  and humidity at  $55\% \pm 10\%$  and subjected to a 12 h day/night cycle with *ad libitum* access to food and water. All animal study procedures were conducted in strict accordance with the guidelines set forth by the Animal Research Institute Committee, as sanctioned by the Institutional Animal Care and Use Committee of Huazhong University of Science and Technology (ethical approval no. 3554).

Mice were divided according to a random number table method into the sham group, sham + luteolin (SL) group, ischemia/reperfusion model (IR) group, and ischemia/reperfusion + luteolin (IL) group. Each group had six mice. The dosage and administration of luteolin in this study followed the methods of previous studies [15–18]. The dose was calculated according to recommended daily intake for humans [19] and modified for mouse physiology. The IL group was given luteolin at 10 mg/

(kg·d) for 7 d before ischemia/reperfusion surgery and for another 3 d after the surgery. The sham group underwent thoracotomy without coronary artery ligation. The IR group underwent thoracotomy and coronary artery ligation. The SL group was administered the same dosage and duration of luteolin as in the IL group without undergoing coronary artery ligation. In the ischemia/reperfusion + luteolin + NSC319726 (ILN) group, NSC319726 at a dose of 10 mg/(kg·d) was administrated from 3 d before the ischemia/reperfusion surgery and continued until 3 d after the surgery. In the ischemia/reperfusion + pifithrin- $\alpha$  (IP $\alpha$ ) group, pifithrin- $\alpha$  (1.1 mg/kg) was administered intraperitoneally every other day, commencing on the 7th day before surgery and was continued until the 3rd day after surgery.

### 2.3. Establishment of the mouse model of MIRI

Myocardial ischemia/reperfusion surgery was performed according to the experimental model guidelines for myocardial ischemia and infarction [20]. The mice were injected with pentobarbital (1%, 40 mg/kg) for anesthesia, restrained in a supine position and ventilated at a respiratory rate of 110 times/min. The mouse chest movements were then monitored to assess breathing and confirm successful intubation. Following meticulous hair removal and sterilization of the surgical area, the thoracotomy was performed to visualize the heart. The left anterior descending coronary artery was ligated with sutures under a microscope and the slipknot was opened 30 min later. After the mice woke up, they were taken off the ventilator and received focused care for 3 d.

### 2.4. Myocardial infarction area detection

After euthanizing the mice 3 d post-ischemia/reperfusion surgery, Evans blue (3%, 1 mL) was injected into the inferior vena cava. The hearts of the mice were excised, frozen, uniformly sectioned along the longitudinal axis into five slices (approximately 2.5 mm in thickness), and sequentially stained with 2% 2,3,5-triphenyltetrazolium chloride (TTC) at  $37^\circ\text{C}$  for 20 min; subsequently they were fixed with 4% paraformaldehyde for 10 min, and photographed. In the stained results, blue indicates the presence of healthy myocardial tissue, red represents the area at risk, and white represents the infarcted region. The areas were measured using Image-Pro Plus 6.0 software (Media Cybernetics, Inc., Rockville, MD, USA) with the percentage of the infarcted area represented as the proportion of the white region to the total heart section area.

### 2.5. Echocardiography

The cardiac functions of mice were assessed using M-mode echocardiography with a Vevo 2100 Imaging System (FUJIFILM VisualSonics, Inc., Toronto, ON, Canada). Two-dimensional targeted M-mode traces were recorded from the parasternal short-axis view at the mid-papillary muscle level and from the parasternal long-axis view below the papillary muscle. A minimum of six consecutive cardiac cycles were obtained. The left ventricular systolic diameter (LVIDs), left ventricular diastolic diameter (LVIDd), left ventricular end diastolic volume (LVEDV), and left ventricular end systolic volume (LVESV) were assessed. The velocities of early diastolic filling peak (E-wave) and late diastolic filling peak (A-wave) of mitral valve blood flow were also examined, along with the E-wave deceleration time (DT). The E/A ratio was the ratio of the E-wave velocity to the A-wave velocity. The left ventricular ejection fraction (LVEF) and the left ventricular fractional shortening (LVFS) were calculated as:

$$LVEF = \frac{LVEDV - LVESV}{LVEDV} \times 100\%.$$

$$LVFS = \frac{LVIDd - LVIDs}{LVIDd} \times 100\%.$$

## 2.6. Detection of myocardial enzymes and oxidative stress indicators

Blood samples were collected 1 d post-ischemia/reperfusion surgery and centrifuged to retain the serum. Serum creatine kinase (CK) and CK muscle/brain subtype (CK-MB) were detected using a CK assay kit (A032-1-1) and CK-MB isoenzyme assay kit (E006-1-1), respectively, from Nanjing Jiancheng Bioengineering Institute (Nanjing, China). The level of cardiac troponin I (cTnI) was assessed using an enzyme-linked immunosorbent assay kit (SEKM-0153, Solarbio, Inc., Beijing, China). Malondialdehyde (MDA), superoxide dismutase (SOD), and glutathione (GSH) were analyzed using assay kits (A003-1-1, A001-3-2, and A006-2-1, Nanjing Jiancheng Bioengineering Institute, Nanjing, China). The detections were conducted following the manufacturers' guidelines.

## 2.7. Prediction of luteolin and MIRI-related target genes

The molecular configuration and simplified molecular input line entry specification of luteolin were acquired from the PubChem database (<https://pubchem.ncbi.nlm.nih.gov/compound/442428>) [21]. Information on targets associated with luteolin was gathered through the Traditional Chinese Medicine Systems Pharmacology (TCMSP, <https://www.tcmsp-e.com/>), SwissTargetPrediction (<https://www.swisstargetprediction.ch/>) [22], and PharmMapper (<https://lilab-ecust.cn/pharmmapper/index.html>) databases. Target designations were standardized through the UniProt database (<https://www.uniprot.org/>) [23].

MIRI-associated target genes were compiled from GeneCard (<https://www.genecards.org/>), Online Mendelian Inheritance in Man (OMIM, <https://omim.org/search/advanced/geneMap>) [24], Pharmacogenetics and Pharmacogenomics Knowledge Base (PharmGkb, <https://www.pharmgkb.org/>), Therapeutic Target Database (TTD, <https://idrblab.net>) [25], and DrugBank (<https://go.drugbank.com/>) [26]. The intersection between luteolin and MIRI-associated targets was visualized with Venny online tool (<https://bioinfogp.cnb.csic.es/tools/venny/index.html>) [27].

## 2.8. Protein-protein interaction network analysis, and molecular docking

The analysis of biofunction properties through Gene Ontology (GO) and the exploration of molecular pathway via the Kyoto Encyclopedia of Genes and Genomes (KEGG) were conducted using packages for the R statistical language environment including “org.hs.eg.db,” “DOSE,” “clusterProfiler,” “Enrichment plot,” “GGplot2,” and “Pathview.” The network depicting protein–protein interaction (PPI) among targets was acquired via the Search Tool for The Retrieval of Interacting Genes/Proteins (STRING) 11.5 (<https://string-db.org/>) [28]. The visualization of the PPI network was produced using Cytoscape 3.9.1 (Cytoscape Consortium, San Diego, CA, USA) [29]. NetworkAnalyzer and CytoNCA plug-ins were used for topological investigation of the PPI network. The 2D structure of luteolin was procured from the PubChem database (<https://pubchem.ncbi.nlm.nih.gov/>) and transmuted into a 3D structure utilizing ChemBio3D Ultra 14.0 (CambridgeSoft, Inc., Cambridge, MA, USA). Molecular docking was conducted with AutoDock Vina v.1.2.0 (The Scripps Research Institute, La Jolla, CA, USA) [30].

## 2.9. Western blotting analysis

To extract the nuclear proteins, the nuclear and cytoplasmic protein extraction kit (P0027, Beyotime Biotech, Inc., Shanghai, China) was used according to the manufacturer's instructions. The right ventricular tissue was isolated and lysed with radioimmunoprecipitation assay lysis buffer, phenylmethylsulfonyl fluoride, and protease inhibitors (Sigma-Aldrich, Inc., St. Louis, MO, USA). The protein content was measured with a bicinchoninic acid (BCA) protein assay kit (P0010, Beyotime Biotech, Inc., Shanghai, China). Lysates were separated electrophoretically on a 10% sodium dodecyl sulfate polyacrylamide gel and transferred onto polyvinylidene difluoride membranes (IPVH00010, Millipore Corporation, Billerica, MA, USA). The membrane was blocked with 5% skimmed milk (232100, BD, Franklin Lakes, NJ, USA) for 1 h, followed by overnight incubation at 4 °C with the following primary antibodies: 1:1000 p53 (A5761), 1:1000 murine double minute 2 (Mdm2, A23388), 1:500 lamin B1 (LmnB1, A11495), 1:1000 caspase 3 (Casp3, A19654), and 1:1000 cleaved Casp3 (A22869) from ABclonal, Inc. (Woburn, MA, USA), 1:1000 B cell lymphoma 2 (Bcl2, TU323153s), 1:1000 Bcl-associated X protein (Bax, Tu33334s), and 1:1000 phosphorylated p53 (p-p53) (Ser15, TP56395) from Abmart Medicine Technology Co., Ltd. (Shanghai, China), and 1:1000 α-actin (23660-1-AP, Proteintech Group, Inc., Rosemont, IL, USA). The membranes were washed in tris-buffered saline with 0.1% Tween (TBST) and immersed in the secondary antibody (AS014, ABclonal, Inc., Woburn, MA, USA) for 1 h at room temperature. The membrane was washed again with TBST and then subjected to enhanced chemiluminescence liquid (G3308, Gbcbio Technologies, Inc., Guangzhou, China) and visualized using the iBright™ CL1500 Imaging System (A44114, Thermo Fisher Scientific, Inc., Waltham, MA, USA).

## 2.10. Real-time quantitative reverse transcription polymerase chain reaction

Total RNA from tissues and cells was extracted using TRIzol reagent (ATG Biotechnology Co., Ltd., Nanjing, China). RNA was then prepared with SynScript® III RT SuperMix for quantitative polymerase chain reaction (qPCR) (+gDNA remover, TSK314S) and 2 × TSINGKE® Master qPCR Mix (SYBR Green I, TSE201) according to the manufacturer's instructions (Tsingke Biotech Co., Ltd., Beijing, China). The detection was conducted using the MA-6000 real-time quantitative thermal cycler (Suzhou Molaray Co., Ltd., Suzhou, China). Relative RNA levels were analyzed with the  $2^{-\Delta\Delta Ct}$  method and β-actin served as an internal benchmark. The primers were listed in Table 1.

## 2.11. Terminal deoxynucleotidyl transferase-mediated dUTP nick-end labeling assay

The one-step terminal deoxynucleotidyl transferase-mediated dUTP nick-end labeling (TUNEL) assay kit (E-CK-A320, Elabscience Bionovation, Inc., Houston, TX, USA) and dihydroethidium (DHE, S0063S, Beyotime Biotech, Inc., Shanghai, China) were used, and the detection was conducted following the manufacturers' instructions.

## 2.12. Reactive oxygen species assays

The measurement of reactive oxygen species (ROS) production in the myocardial tissues was conducted with DHE (S0063S, Beyotime Biotech, Inc., Shanghai, China). The myocardial tissues were washed with PBS and then incubated with DHE (5 μmol/L) at 37 °C for 30 min. A fluorescence microscope (BX50, Olympus Corporation, Tokyo, Japan) was used to assess fluorescence intensity.

**Table 1**

The primer sequences.

Gene	Forward sequence	Reverse sequence	Product length (bp)
<i>β</i> -Actin	5'-GGCTGTATTCCCCCTCCATCG-3'	5'-CCAGTTGGAACCATGCCATGT-3'	153
<i>Mdm2</i>	5'-CAGTAGCAGTGAATCTACAGGGA-3'	5'-CTGATCCAACCAATCACCTGAAT-3'	107
<i>Trp53</i>	5'-CTCTCCCCCGCAAAAGAAAAA-3'	5'-CGAACATCTCGAAGCGTTA-3'	84

Mdm2: murine double minute 2; Trp53: transformation related protein 53.

The ROS production in HL1 cells was measured with an ROS assay kit (S0033S, Beyotime Biotech, Inc., Shanghai, China). HL1 cells were washed with PBS three times and then incubated with the fluorescent probe 2,7-dichlorodihydrofluorescein diacetate (DCFH-DA, 10 μmol/L) at 37 °C for 30 min. Cells were acquired and analyzed using a CytoFLEX™ flow cytometer (Beckman Coulter, Inc., Brea, CA, USA).

### 2.13. Cell culture and cell viability analysis

The murine cardiac muscle cell line (HL1) was purchased from Procell Life Science & Technology Co., Ltd. (CL-06-5, Wuhan, China). To establish the hypoxia/reoxygenation (HR) model, HL1 cells were cultured under hypoxic conditions of 95% N<sub>2</sub> + 5% CO<sub>2</sub> for 12 h at 37 °C. The cells were then relocated to a normoxic incubation at 37 °C for 6 h of reoxygenation. The normal control group was cultivated within a conventional incubator setting. In the 6-hour reoxygenation, the HR model group was incubated with PBS, the HR + luteolin group was incubated with luteolin, and the HR + luteolin + NSC group was incubated with 10 μmol/L NSC319726.

The HL1 cells were nurtured in 96-well plates (1 × 10<sup>4</sup> cells/well). In brief, 10 μL Cell Counting Kit-8 (CCK-8) reagent (GK10001, GlpBio Technology, Montclair, CA, USA) was added to each well and incubated with cells for an extra 40 min. The absorbance was measured at a wavelength of 450 nm with Infinite® F50 Plus microplate reader (Tecan Group Ltd., Männedorf, Switzerland).

### 2.14. Cell apoptosis assay

Cell apoptosis was measured using flow cytometry with the Annexin V-fluorescein isothiocyanate (FITC)/propidium iodide (PI) apoptosis kit (AP101, Lianke Biotech, Co., Ltd, Hangzhou, China). Briefly, the HL1 cells were collected after treatment, and then rinsed with PBS for binding and staining. The cells were examined under a CytoFLEX™ flow cytometer (Beckman Coulter, Inc., Brea, CA, USA).

### 2.15. JC-1 assay

5,5',6,6'-Tetrachloro-1,1',3,3'-tetraethylbenzimi-dazoylcarbo cyanine iodide (JC-1) fluorescence detection was conducted using the JC-1 mitochondrial membrane potential assay kit (C2006, Beyotime Biotech, Inc., Shanghai, China), followed by fluorescence imaging analysis using a fluorescence microscope (BX50, Olympus Corporation, Tokyo, Japan). Meanwhile, the JC-1 detection was also conducted with flow cytometry. The HL1 cells were stained with JC-1 staining solution. Subsequently, the CytoFLEX™ flow cytometer was employed for fluorescence analysis of the cells.

### 2.16. Statistical analysis

GraphPad Prism 8.2.1 (GraphPad Software, Boston, MA, USA) was used for statistical analyses. Data are presented as mean ± standard error of the mean. The two-tailed Student's *t* test

was used for comparisons between two groups. For multiple comparisons, one-way analysis of variance test was applied. The comparison between the two groups was performed by unpaired *t*-test. *P*-value < 0.05 indicates statistical significance.

## 3. Results

### 3.1. Luteolin decreased myocardial infarction area and enzyme levels and reinstated cardiac function after MIRI *in vivo*

To assess the therapeutic efficacy of luteolin against MIRI, luteolin was administered to MIRI mice, and the myocardial enzymes, myocardial infarct size, and cardiac contractility of mice were examined. The size of infarcts in myocardial tissue was evaluated using Evans blue and TTC dual staining. Fig. 1A and 1B illustrate the reduction in the extent of infarctions within the IL group, compared to the IR group. Serum CK, CK-MB, and cTnI levels were elevated in the IR group relative to the sham group. Administration of luteolin reduced serum CK, CK-MB, and cTnI concentrations in the mice of the IL group compared to the IR group (Fig. 1C). The echocardiographic findings revealed notable reductions in LVEF and LVFS among the IR group in contrast to the sham group. Conversely, the IL group exhibited heightened levels of these two indicators in contrast to the IR group, implying the restoration of myocardial contractile power in mice subjected to ischemia/reperfusion injury (Fig. 1D and 1E). Luteolin also significantly improved LVIDd and LVIDs in the IR group (Fig. 1D and 1E), but did not improve the E/A ratio or the DT of the mitral valve (Supplementary figure S1). In contrast with the sham group, the provision of luteolin to mice subjected to the sham operation did not induce any modification in the area of the infarct, cardiac enzymes, or cardiac function, indicating that luteolin did not have significant toxic side effects in the mice (Fig. 1). Collectively, these findings showed that luteolin exerts a protective function in MIRI.

### 3.2. p53 was identified as the potential target of luteolin

The oral bioavailability and drug-likeness of luteolin were greater than 30% and 0.18, respectively (Supplementary Table S1), which indicated that luteolin had a good drug-likeness [31,32]. To further study the pharmacological effects of luteolin, the TCMSp, SwissTargetPrediction, and PharmMapper databases were used to discern the targets of the constituents of the drug. A total of 169 predicted target genes of luteolin were identified by screening and further verified (Supplementary Table S2). Next, the GeneCards, DrugBank, OMIM, PharmGkb, and TTD databases were used to find MIRI-related target genes, and a total of 3176 genes were identified (Fig. 2A). There were 104 overlapping genes between luteolin-related target genes and MIRI-related ones, and this was considered to be the possible target set for luteolin in MIRI treatment (Fig. 2B and Supplementary Table S3).

The GO and KEGG enrichment analyses were conducted to investigate the biological function of the 104 common target genes shared by luteolin and MIRI. GO analysis yielded a total of 1749 biological processes (BPs), 55 cell components (CCs), and 153 molecular functions (MFs). The top five markedly enriched BPs,

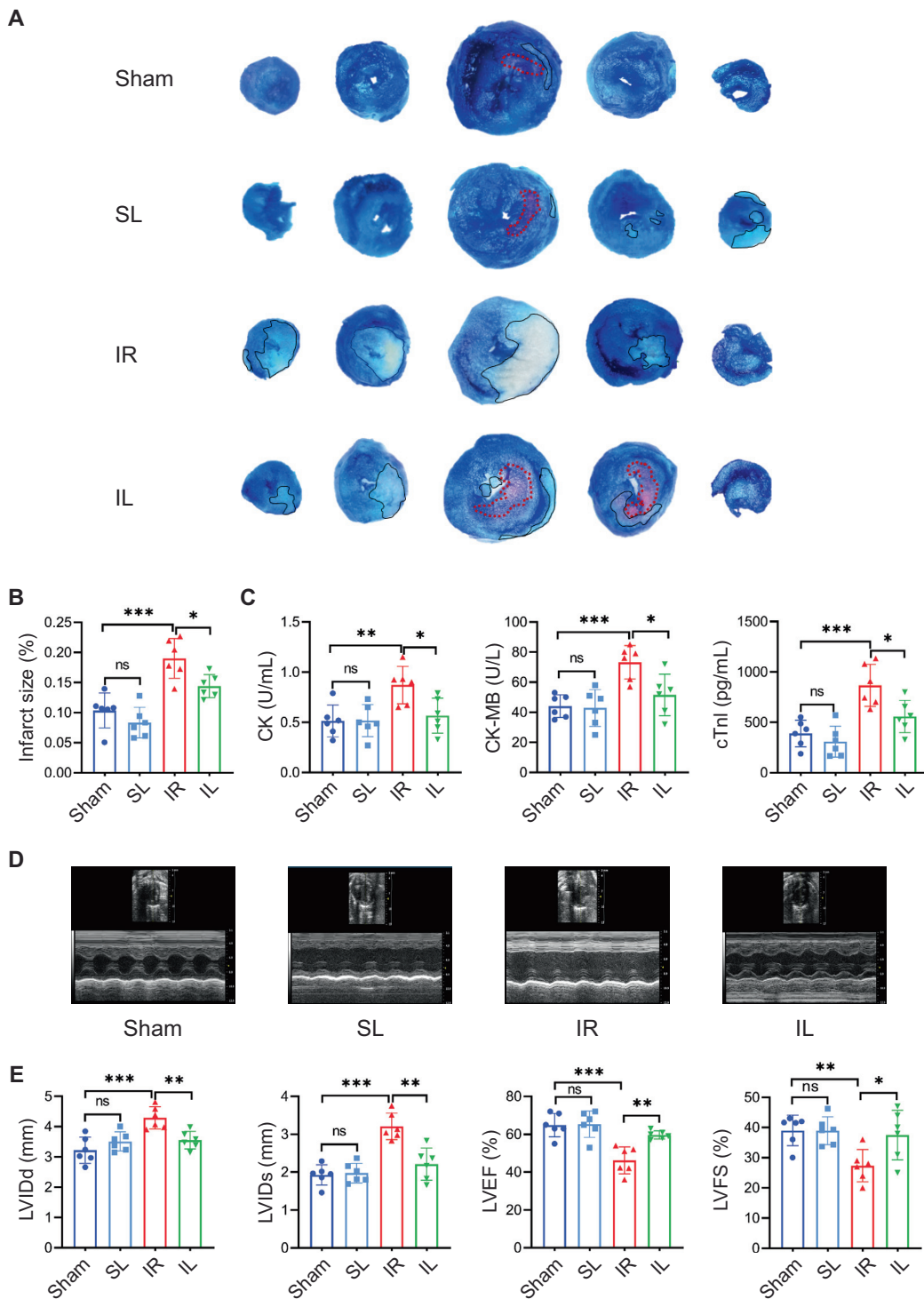


**Fig. 1.** Luteolin protected against MIRI in vivo. (A) Representative digital images of heart sections visualized with Evans blue and TTC double staining. The blue-stained portion indicates the normal region, the red-stained portion, outlined in red, indicates the ischemic region, and the white portion, outlined in black, indicates the infarcted region. (B) Percentage of infarct area. The ratio of the infarct area of the largest heart section to the total area of the section was used to calculate the infarct percentage. (C) Serum CK, CK-MB, and cTnI levels. (D) Representative M-mode echocardiographic images. (E) Quantitative statistical analysis of LVIDd, LVIDs, LVEF, and LVFS. CK: creatine kinase; CK-MB: CK muscle/brain subtype; cTnI: cardiac troponin I; IL: ischemia/reperfusion + luteolin; IR: ischemia/reperfusion; LVEF: left ventricular ejection fraction; LVFS: left ventricular fractional shortening; LVIDd: left ventricular systolic diameter; LVIDs: left ventricular diastolic diameter; MIRI: myocardial ischemia/reperfusion injury; SL: sham + luteolin; TTC: 2,3,5-triphenyltetrazolium chloride. Data are presented as mean  $\pm$  standard error of the mean,  $n = 6$ . ns: not significant; \* $P < 0.05$ , \*\* $P < 0.01$ , and \*\*\* $P < 0.001$ .

CCs, and MFs are presented in Fig. 2C. The target genes for “response to oxidative stress” were the most enriched gene sets among all the target genes. To ascertain the potential signaling

pathways involved in luteolin-mediated protection in MIRI, the KEGG pathway enrichment analysis was used to scrutinize the top 20 signaling pathways (Fig. 2D). We discovered that apoptosis

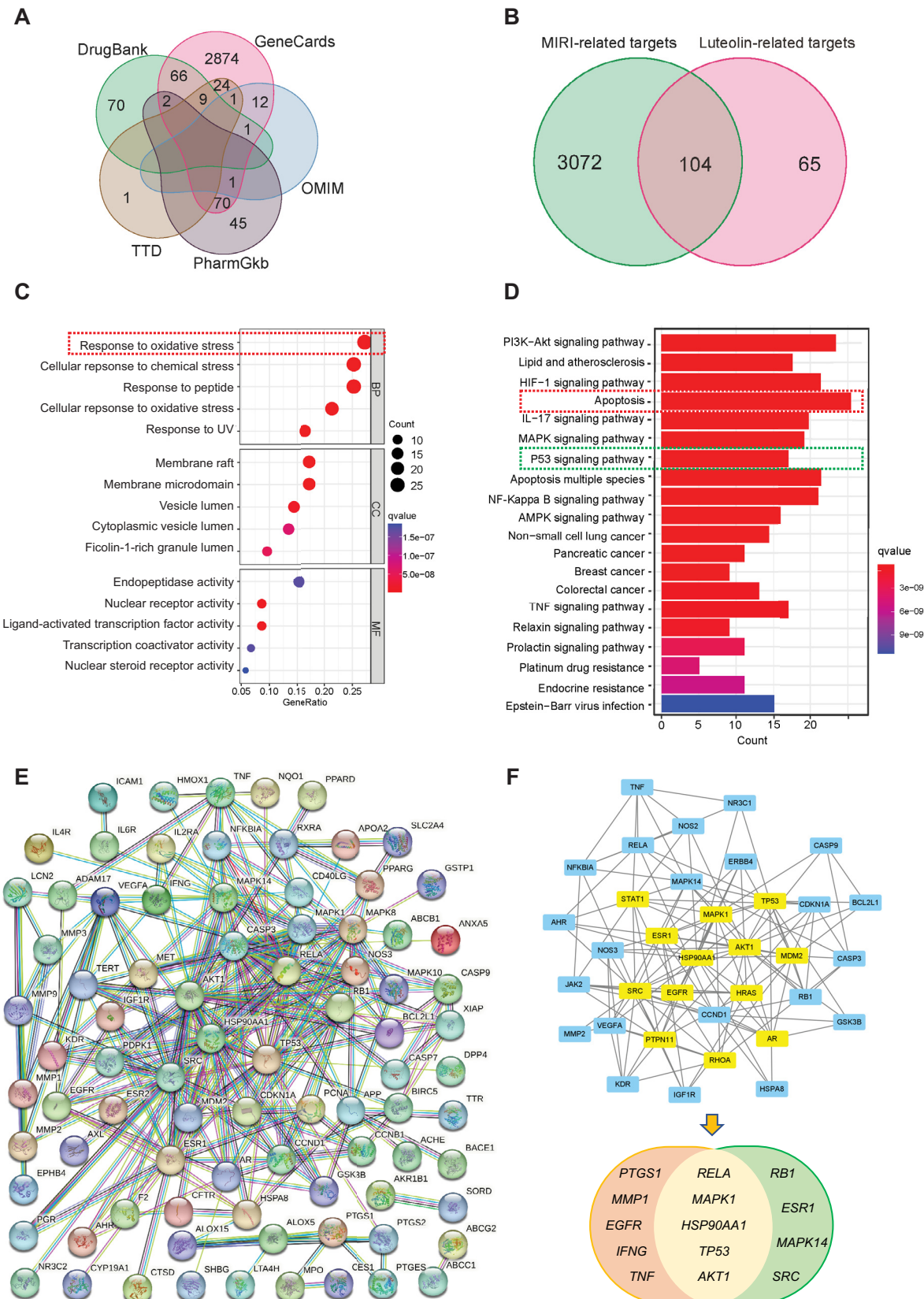


**Fig. 2.** Luteolin has the potential to target p53 in the treatment of MIRI. (A) The overlap among MIRI-related target genes returned from different databases. (B) The intersection of MIRI-related and luteolin-related targets. (C) GO enrichment analysis of the targets of luteolin in the treatment of MIRI. (D) KEGG pathway enrichment analysis of the targets of luteolin in the treatment of MIRI. (E) Protein-protein interaction network analysis of the targets of luteolin in the treatment of MIRI. In the network, circular nodes represent proteins, and the lines represent the interactions between the proteins. (F) Topological analysis and hub targets of luteolin in the treatment of MIRI. BP: biological process; CC: cell component; GO: Gene Ontology; KEGG: Kyoto Encyclopedia of Genes and Genomes; MF: molecular function; MIRI: myocardial ischemia/reperfusion injury.

and p53 signaling pathways were the most related to cell death. Therefore, we hypothesized that luteolin may manifest cardioprotective properties by attenuating oxidative stress or apoptosis.

To assess the interplay between luteolin and MIRI common targets, the PPI network analysis was performed. The cohort of 104 shared targets were imported into the STRING 11.5 database, and a combined score  $\geq 0.9$  was set as the threshold. The network comprises 85 nodes interconnected by 261 edges, yielding an average degree of 6.14. The AKT serine/threonine kinase 1 (*AKT1*), heat shock protein 90  $\alpha$  family class A member 1 (*HSP90AA1*), mitogen-activated protein kinase 1 (*MAPK1*), RELA proto-oncogene (*RELA*), and tumor protein p53 (*TP53*), were strongly connected to others (Fig. 2E and Supplementary figure S2). Then, the PPI network was imported into the Cytoscape, and topology analysis was used to identify the hub targets from these interacting proteins. Nine hub targets were screened, namely *AKT1*, *HSP90AA1*, *MAPK1*, *MAPK14*, *RELA*, *TP53*, estrogen receptor 1 (*ESR1*), SRC proto-oncogene (*SRC*), and RB transcriptional corepressor 1 (*RB1*) (Fig. 2F).

Next, a luteolin-MIRI-target-GO-KEGG pathway network was constructed (Fig. 3). The targets were ranked from highest to lowest based on the degree of the network topology analysis parameters. *TP53*, *MAPK1*, *RELA*, *AKT1*, *HSP90AA1*, interferon  $\gamma$  (*IFNG*), epidermal growth factor receptor (*EGFR*), tumor necrosis factor (*TNF*), matrix metallopeptidase 1 (*MMP1*), and prostaglandin-endoperoxide synthase 1 (*PTGS1*) had the highest scores. The intersection of these 10 targets with the nine hub genes obtained from the PPI analysis (Fig. 2F) yielded five key genes, namely *TP53*, *HSP90AA1*, *AKT1*, *MAPK1*, and *RELA*.

Previous investigations have indicated that luteolin mitigates myocardial damage through regulating the phosphoinositide-3-

kinase (PI3K)-AKT [33], MAPK [12], and nuclear factor- $\kappa$ B (NF- $\kappa$ B) pathways [17,25]; however, whether luteolin can regulate p53 and HSP90 pathways to prevent MIRI has not yet been studied. Moreover, the p53 signaling cascade emerged as a pivotal pathway in the KEGG assessment of luteolin intervention in MIRI (Fig. 2D). Therefore, the p53 pathway was selected for further investigation.

### 3.3. Luteolin alleviated myocardial cell apoptosis and oxidative stress caused by MIRI

To evaluate the biological activity and the binding affinity of luteolin to p53 protein, molecular docking analysis was performed. Luteolin has multiple possible binding sites with p53, with the lowest binding energy being  $-5.4$  kcal/mol, indicating an excellent strong affinity between luteolin and p53 (Fig. 4A). Mdm2 is a pivotal protein within the intricate framework of the p53 signaling pathway. Mdm2 promotes p53 degradation while restraining transcriptional activity. The levels of mRNA for *p53* and *Mdm2* within the ischemia/reperfusion cardiac tissue were markedly elevated in comparison to those in the sham group. However, following luteolin administration, there was a decline in *p53* mRNA expression juxtaposed with an escalation in *Mdm2* mRNA expression (Fig. 4B). A similar tendency was detected in the protein level, with a notable increase in the expression of nuclear protein p-p53 observed in the IR group. Conversely, luteolin treatment decreased the expression of p-p53 (Fig. 4C). These data illustrated that luteolin had facilitated the upregulation of Mdm2 and had suppressed the production of p53, whether at the protein or mRNA level. This implied that luteolin had protected against myocardial injury by impeding the p53 pathway.

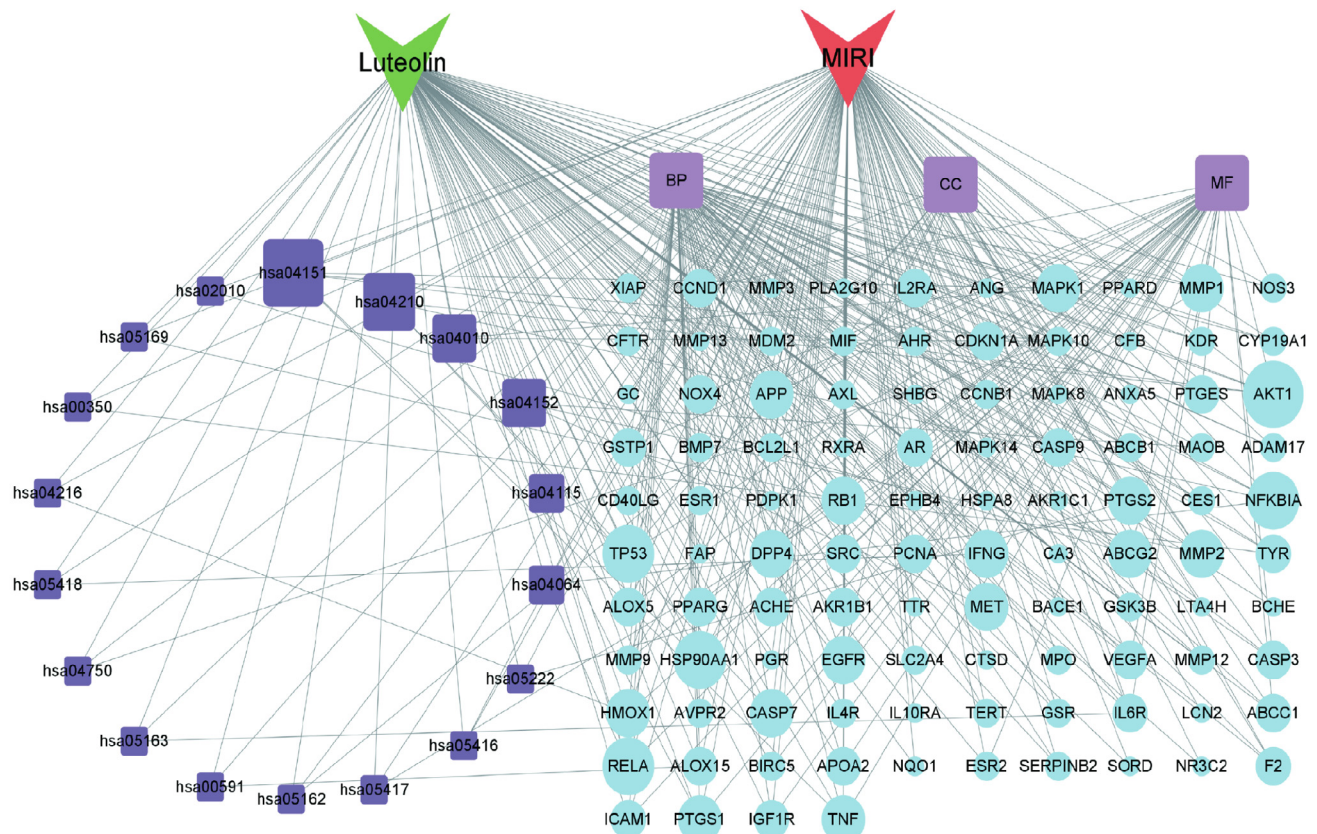


**Fig. 3.** The luteolin-MIRI-target-GO-KEGG pathway network. BP: biological process; CC: cell component; GO: Gene Ontology; KEGG: Kyoto Encyclopedia of Genes and Genomes; MF: molecular function; MIRI: myocardial ischemia/reperfusion injury.

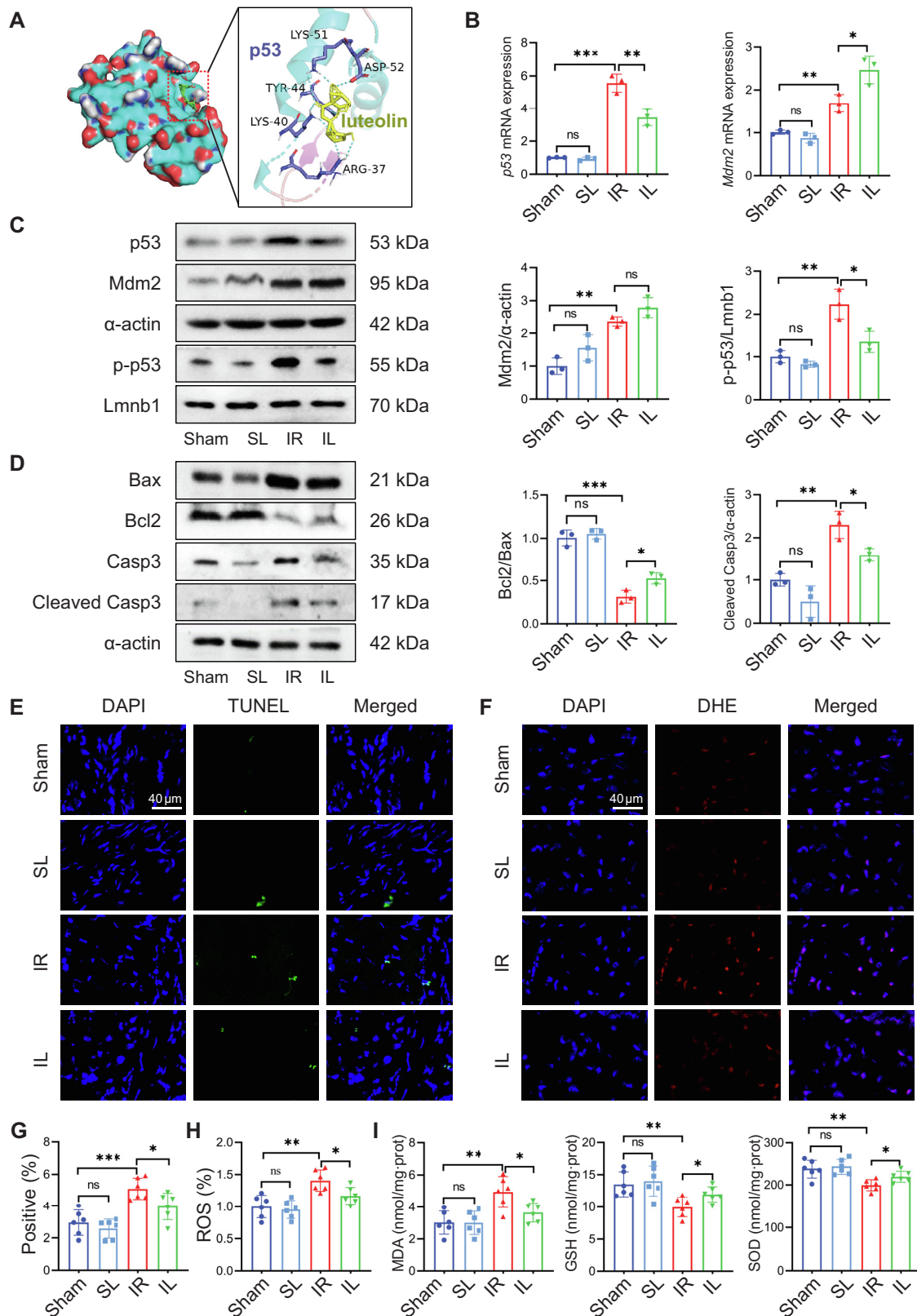


**Fig. 4.** Luteolin regulates the p53 signaling pathway and inhibits apoptosis and oxidative stress in MIRI. (A) The docking of p53 protein and luteolin. (B) Quantitative analysis of p53 and Mdm2 mRNA expression. (C) Representative blots of p53, Mdm2, and the nuclear protein p-p53 in myocardial tissue and quantification of p-p53 and Mdm2 expression. (D) Representative blots of Bax, Bcl2, Casp3, and cleaved Casp3 and quantification of Bax and cleaved Casp3 expression. (E) Representative images of apoptotic cardiomyocytes ( $40\times$  magnification). The apoptotic cells were detected by TUNEL (green) and the nuclei were detected by DAPI (blue). (F) Representative images of oxidative stress in cardiomyocytes ( $40\times$  magnification). ROS was detected with DHE fluorescence staining (red) and nuclei were detected with DAPI (blue). (G) The quantitative analysis of the TUNEL<sup>+</sup> cells. (H) The quantitative analysis of the ROS levels. (I) The quantitative analysis of myocardial MDA content and GSH and SOD activity. Box: Bcl2-associated X protein; Bcl2: B cell lymphoma 2; Casp3: caspase 3; DAPI: 4',6-diamidino-2-phenylindole; DHE: dihydroethidium; GSH: glutathione; I/R: ischemia/reperfusion; IL: ischemia/reperfusion + luteolin; LmnB1: lamin B1; MDA: malonaldehyde; Mdm2: murine double minute 2; ROS: reactive oxygen species; SL: sham + luteolin; SOD: superoxide dismutase; TUNEL: terminal deoxynucleotidyl transferase-mediated dUTP nick-end labeling. Data are presented as mean  $\pm$  standard error of the mean,  $n = 6$ . ns: not significant; \* $P < 0.05$ , \*\* $P < 0.01$ , and \*\*\* $P < 0.001$ .

Based on the GO and KEGG analyses, it is suggested that the regulation of apoptosis and oxidative stress potentially serves as the dominant mechanisms through which luteolin exerts its cardioprotective effects. The upregulation of Bax and cleaved Casp3 was noted in the IR group relative to the sham group. After luteolin administration, there was a notable increase in Bcl2 expression and the Bcl2/Bax ratio, while the expression of cleaved Casp3 protein was lower than in the IR group (Fig. 4D). Moreover, the quantity of TUNEL<sup>+</sup> cells in the myocardial tissue was markedly diminished in the IL group when compared to the IR group, indicating that luteolin prevented myocardial apoptosis caused by MIRI (Fig. 4E and 4G). The fluorescence intensity indicated that the intracellular superoxide level was diminished in the IL group compared with the IR group (Fig. 4F and 4H). Additionally, luteolin treatment reduced MDA levels that were elevated by ischemia/reperfusion, and increased activities of GSH and SOD that were reduced by ischemia/reperfusion (Fig. 4I). These observations indicated that luteolin mitigated the oxidative stress in myocardial tissue that was caused by MIRI.

#### 3.4. Luteolin mitigated HR-induced apoptosis and oxidative stress responses through regulating p53 in vitro

The effect of luteolin on the survival of HL1 cells under normal oxygen conditions was assessed. Luteolin of 5, 10, and 20 μmol/L exhibited negligible influence on HL1 cells compared to the normal control group (Supplementary figure S3A). Then, the therapeutic effect of luteolin on HL1 cells incubated with HR was evaluated, revealing that luteolin augments HL1 cell viability in a dose-dependent fashion (Supplementary figure S3B). Next, the apoptotic cells underwent analysis through Annexin V-FITC/PI staining. The proportion of apoptotic cells in the HR + luteolin group markedly decreased compared to that of the HR group, indicating that luteolin alleviated HR-induced apoptosis of HL1 cells. However, the efficacy of luteolin in reducing HR-induced apoptosis was reversed after administration of NSC319726, an agonist of p53 (Fig. 5A), indicating that luteolin exerts an anti-apoptotic effect by inhibiting p53. Luteolin decreased the expression of HR-mediated p53 and p-p53 proteins, as well as the apoptosis related proteins, Bax and cleaved Casp3 (Fig. 5B). In addition, luteolin administration increased the level of anti-apoptosis protein Bcl2, as well as the Bcl2/Bax ratio (Fig. 5C). Nevertheless, the NSC319726 intervention upregulated apoptosis-related proteins. The analysis of JC-1 fluorescence staining and flow cytometry revealed that HR treatment leads to a relative increase in JC-1 monomers compared to aggregates (Fig. 5D and 5E), and treatment with luteolin resulted in a reduced HR-induced monomer content relative to the JC-1 aggregate content. Notably, the addition of the p53 agonist reversed the beneficial effects of luteolin (Fig. 5F). These observations strongly suggested that luteolin effectively ameliorates mitochondrial dysfunction induced by HR through p53.

The flow cytometry analysis showed that luteolin reversed HR-mediated upregulation of DCF expression, which indicated that luteolin suppressed the oxidative stress response in MIRI (Fig. 5G). In addition, luteolin reversed the heightened fluorescence intensity of DHE induced by HR. The p53 activator NSC319726 induced an increase in the concentration of DHE<sup>+</sup> cells, despite the intervention with luteolin (Fig. 5H and 5I). Furthermore, the HR group exhibited greater levels of oxidative stress, and luteolin successfully mitigated this stress, as shown by the decreased MDA content and the restoration of GSH and SOD activities (Fig. 5J). These findings show that luteolin alleviated the oxidative stress caused by HR. However, when using the p53 activator, the ability of luteolin to combat oxidative stress was diminished. These results establish that luteolin exerts its anti-apoptotic and anti-oxidative stress properties by specifically targeting p53.

#### 3.5. Luteolin exerted a cardioprotective effect on MIRI mice by modulating the p53 pathway

To determine whether luteolin could protect cardiomyocyte from MIRI by regulating the p53 pathway, we treated MIRI mice with the p53 agonist, NSC319726, and the p53 inhibitor, pifithrin-α, and evaluated the extent of infarction, myocardial enzyme levels, and cardiac functionality in mouse hearts. The outcomes of Evans blue/TTC dual staining showed a notably larger myocardial infarction zone within the ILN group in contrast to the IL group. Additionally, the infarct region in the IP $\alpha$  group exhibited a notable reduction relative to the IR group, and the difference between infarct area in the IL and IP $\alpha$  groups was not significant (Fig. 6A and 6B). Furthermore, the serum concentrations of CK, CK-MB, and cTnI showed a decline after the administration of luteolin or pifithrin-α. However, the addition of NSC319726 resulted in weakening of luteolin's ability to reduce myocardial enzymes (Fig. 6C). Mice from the IL group or the IP $\alpha$  group showed significant improvements in LVEF, LVFS, LVIDd, and LVIDs, compared to the IR group. Moreover, the administration of NSC319726 resulted in an augmentation of LVIDd and LVIDs, alongside a decrease in LVEF and LVFS, thereby inducing a decline in cardiac systolic function, compared to the IL group. Furthermore, administration of pifithrin-α showed no significant difference compared to luteolin treatment (Fig. 6D and 6E). In terms of assessing cardiac diastolic function, we observed that NSC319726, pifithrin-α, and luteolin had no notable effects on the mitral valve, the ratio of E/A, or the deceleration time of the E-wave (Supplementary figure S4). Taken together, these data showed that luteolin improved the cardiac dysfunction in MIRI mice by mediating the p53 pathway.

## 4. Discussion

Luteolin is a promising agent for alleviating pathological cardiac hypertrophy and cardiac dysfunction [34] through its powerful anti-apoptosis [9] and antioxidant [16] effects. The function of luteolin in MIRI and its potential mechanism remain not yet fully clarified. In this study, luteolin was shown to diminish myocardial infarction size and myocardial enzymes and to reinstate myocardial contractile capacity in mice, confirming the therapeutic effectiveness of luteolin on MIRI.

Cardiomyocytes are rich in mitochondria [35]. MIRI can impair mitochondrial function, subsequently affecting the energy metabolism and redox homeostasis of cardiomyocytes, while also leading to excessive generation of ROS [36,37]. Previous studies have suggested that luteolin can inhibit mitochondrial dysfunction induced by mitochondrial toxins [38], restore mitochondrial membrane potential, preserve overall mitochondrial function, and alleviate oxidative stress [39] in Alzheimer's disease. In this study, luteolin was also found to attenuate the increase in mitochondrial membrane potential elevation caused by HR in HL1 cells and mitigate the excess ROS and the intense oxidative stress response.

Network pharmacological analysis showed that p53 served as a hub target for luteolin in mitigating MIRI. Molecular docking investigations further illustrated that luteolin exhibited a pronounced affinity for p53 binding. Normally, p53 is localized in the cytoplasm of mouse cardiomyocytes; however, under HR condition, p53 expression was markedly elevated and translocated to the nucleus [40], impacting myocardial systolic function [5]. Inhibiting the upregulation and nuclear translocation of p53 was shown to significantly reduce apoptosis in anoxic and reoxygenated cardiomyocytes [40,41]. In our experiments, MIRI indeed induced cardiomyocyte apoptosis and ROS production and concurrently increased the expression and phosphorylation of p53. Luteolin was able to suppress the expression and phosphorylation of p53,

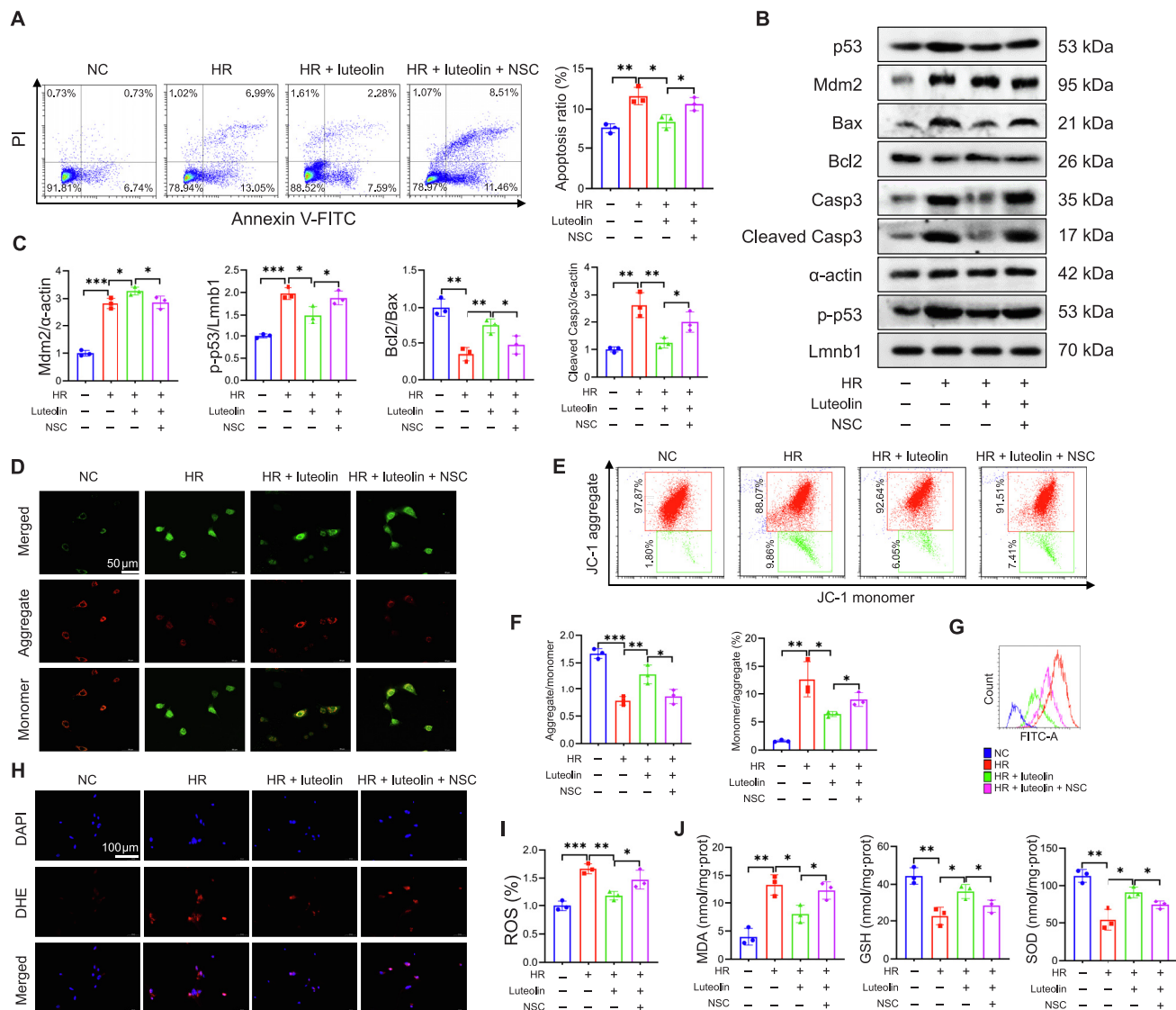


**Fig. 5.** Luteolin alleviated the HR-induced damage of HL1 cells by regulating p53. (A) Representative images of HL1 cell apoptosis detected by flow cytometry and quantitative analysis. (B) Representative Western blots of Bax, Bcl2, cleaved Casp3, p53, p-p53, and Lmnb1 proteins in HL1 cells. (C) Quantification of blots. (D) Representative images of JC-1 fluorescent staining. The red color represents JC-1 aggregates, while the green color represents JC-1 monomers visualized with flow cytometry. (E) Representative images of JC-1 aggregates and monomers. (F) Quantification of JC-1 analyses. (G) The superimposed image depicts the fluorescence intensity of DCF in HL1 cells. (H) Representative image of ROS staining. (I) Quantification of ROS. (J) Cellular MDA content and GSH and SOD activity of HL1 cells. Bax: BCL2-associated X protein; Bcl2: B cell lymphoma 2; Casp3: caspase 3; DAPI: 4',6-diamidino-2-phenylindole; DCF: 2,7-dichlorodihydrofluorescein; DHE: dihydroethidium; FITC: fluorescein isothiocyanate; GSH: glutathione; HR: hypoxia/reoxygenation; HR + luteolin: hypoxia/reoxygenation + luteolin; HR + luteolin + NSC: hypoxia/reoxygenation + luteolin + NSC319726; Lmnb1: lamin B1; MDA: malondialdehyde; Mdm2: murine double minute 2; NC: normal control; NSC: the p53 agonist NSC319726; PI: propidium iodide; ROS: reactive oxygen species; SOD: superoxide dismutase; TUNEL: terminal deoxynucleotidyl transferase-mediated dUTP nick-end labeling. Data are presented as mean  $\pm$  standard error of the mean,  $n = 3$ . \* $P < 0.05$ , \*\* $P < 0.01$ , and \*\*\* $P < 0.001$ .

thereby reducing myocardial infarction area and enzymes, and restoring cardiac contractility. However, when a p53 agonist was administered, the cardioprotective effect of luteolin diminished, indicating that the target of luteolin's cardio-protection is p53.

Luteolin had a protective effect when used to treat endometritis through its inhibition of the activation or phosphorylation of p53 [42]. Moreover, luteolin attenuated p53 induced apoptosis in hepatic tissue [43], obesity [44], and heart failure ailments [45]. However, conflicting results have been observed in human colon cancer, where luteolin promoted and activated p53 expression [46,47]. This may be attributed to disease or tissue specificity, drug administration, and biological complexity. Our results showed that luteolin suppressed p-p53 activation by reducing p53 expression and accumulation, leading to a decrease in MIRI, aligning with the results of other studies investigating non-tumor diseases.

p53 induces cell apoptosis by regulating Bax, Bcl2, phorbol-12-myristate-13-acetate-induced protein 1, and myeloid cell leukemia 1 expression [48,49]. The excessive activation of the p53 pathway initiates a cascade of ROS related gene activations [50,51]. p-p53 can also suppress the transcription of antioxidant genes [52]. Furthermore, oxidative stress can facilitate cellular apoptosis [53]. Upon ROS stimulation, p53 protein was translocated to the mitochondrial membrane and facilitated the accelerated opening of membrane pores, leading to a decrease in membrane potential, and exacerbation of the malignant loop of mitochondrial damage, oxidative stress, and cellular apoptosis [54]. In our study, luteolin treatment reduced apoptosis and ROS level in myocardium with MIRI, accompanied by the decrease of p53. When the p53 agonist was added, luteolin's ability to reduce apoptosis and oxidative stress was diminished; further, the p53 inhibitor exerted a similar

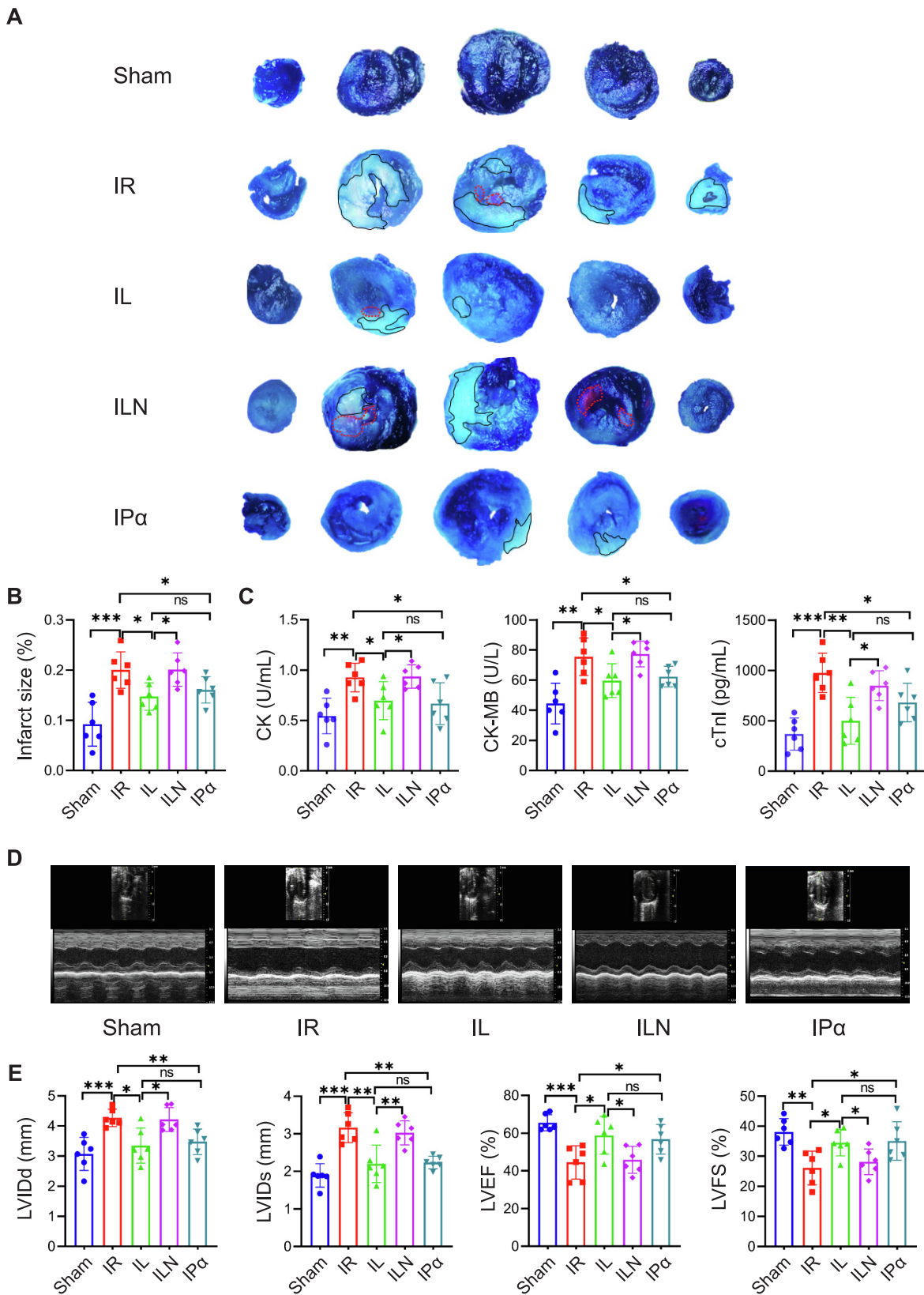


**Fig. 6.** Luteolin exerted a myocardial protective effect regulated by p53. (A) Representative images of heart sections with Evans blue and TTC double staining. (B) The percentage of the infarct area. The ratio of the infarct area of the largest heart section to the section's total area was used to calculate the percentage of infarct area. (C) The serum CK, CK-MB, and cTnI levels. (D) Representative M-mode echocardiographic images. (E) LVDD, LVIDs, LVEF, and LVFS. CK: creatine kinase; CK-MB: CK muscle/brain subtype; cTnI: cardiac troponin I; IL: ischemia/reperfusion group; ILN: ischemia/reperfusion + luteolin + NSC319726; IP $\alpha$ : ischemia/reperfusion + pifithrin- $\alpha$ ; IR: ischemia/reperfusion; LVEF: left ventricular ejection fraction; LVFS: left ventricular fractional shortening; LVIDs: left ventricular systolic diameter; LVDD: left ventricular diastolic diameter; MIRI: myocardial ischemia/reperfusion injury; TTC: 2,3,5-triphenyltetrazolium chloride. Data are presented as mean  $\pm$  standard error of the mean,  $n = 6$ . ns: not significant; \* $P < 0.05$ , \*\* $P < 0.01$ , and \*\*\* $P < 0.001$ .

mitigation of apoptosis and oxidative stress as luteolin, suggesting that the p53 pathway serves as a crucial route through which luteolin mitigates apoptosis and oxidative stress in myocardial cells.

Nevertheless, the precise regulatory effects of luteolin on p53 subunits remain to be further elucidated. For instance, integrating molecular dynamics simulations with mutation analyses to sequentially alter luteolin's binding sites on the p53 protein substructure could provide deeper insights into the mechanistic role of luteolin with respect to p53. Moreover, the manner by which luteolin improves mitochondrial oxidative stress via the p53 signaling pathway still requires clarification, including whether it acts through mitochondrial membrane fusion and fission or through cellular energy metabolism. To this end, elucidating luteolin's mechanisms through mitochondrial function assessments, gene expression analyses, and proteomics studies would lay a scientific foundation for its application in treating cardiovascular disorders.

This study suggests that luteolin can reduce apoptosis and oxidative stress by suppressing p53 expression, thus alleviating myocardial damage in MIRI (Fig. 7). However, the specific regulation of the p53 protein subunit by luteolin remains to be further confirmed. Whether luteolin affects other downstream signaling pathways after modulating the p53 signaling pathway also needs to be further investigated.

## 5. Conclusion

This study investigated the therapeutic efficacy and fundamental mechanism of luteolin on MIRI. Luteolin shielded mice from MIRI, as indicated by the decreased myocardial infarct size and myocardial enzyme levels and augmented systolic function. The results of in vivo and in vitro experiments show that luteolin diminished p53 expression and impeded nuclear translocation of p-p53, thereby averting ROS generation and reducing cellular apoptosis. It is suggested that luteolin mitigated cellular apoptosis and oxidative stress by inhibiting phosphorylation of p53 to alleviate MIRI. This study validates luteolin's potential as a natural drug for MIRI therapy.

## Funding

This work was financially supported by grants from the National Natural Science Foundation of China (No. 82104488, 81974249, 82274317, and 82161138003).

## CRediT authorship contribution statement

PZ conceived the project, analyzed and visualized the data, and drafted the manuscript. PZ, XHO, and MLY conducted the experiments. LL, YML, JYL, and XC revised the manuscript. RZ conceived and administrated the project and revised the manuscript. DSH supervised, administrated the project, revised the manuscript, and acquired funding. All authors read and approved the final manuscript.

## Acknowledgment

The authors would like to thank the National Natural Science Foundation of China.

## Declaration of competing interests

The authors declare that there is no conflict of interest.

## Appendix A. Supplementary material

Supplementary data to this article can be found online at <https://doi.org/10.1016/j.joim.2024.09.001>.

## References

- [1] Reed GW, Rossi JE, Cannon CP. Acute myocardial infarction. *Lancet* 2017;389(10065):197–210.
- [2] Ibanez B, James S, Agewall S, Antunes MJ, Bucciarelli-Ducci C, Bueno H, et al. 2017 ESC Guidelines for the management of acute myocardial infarction in patients presenting with ST-segment elevation: the Task Force for the

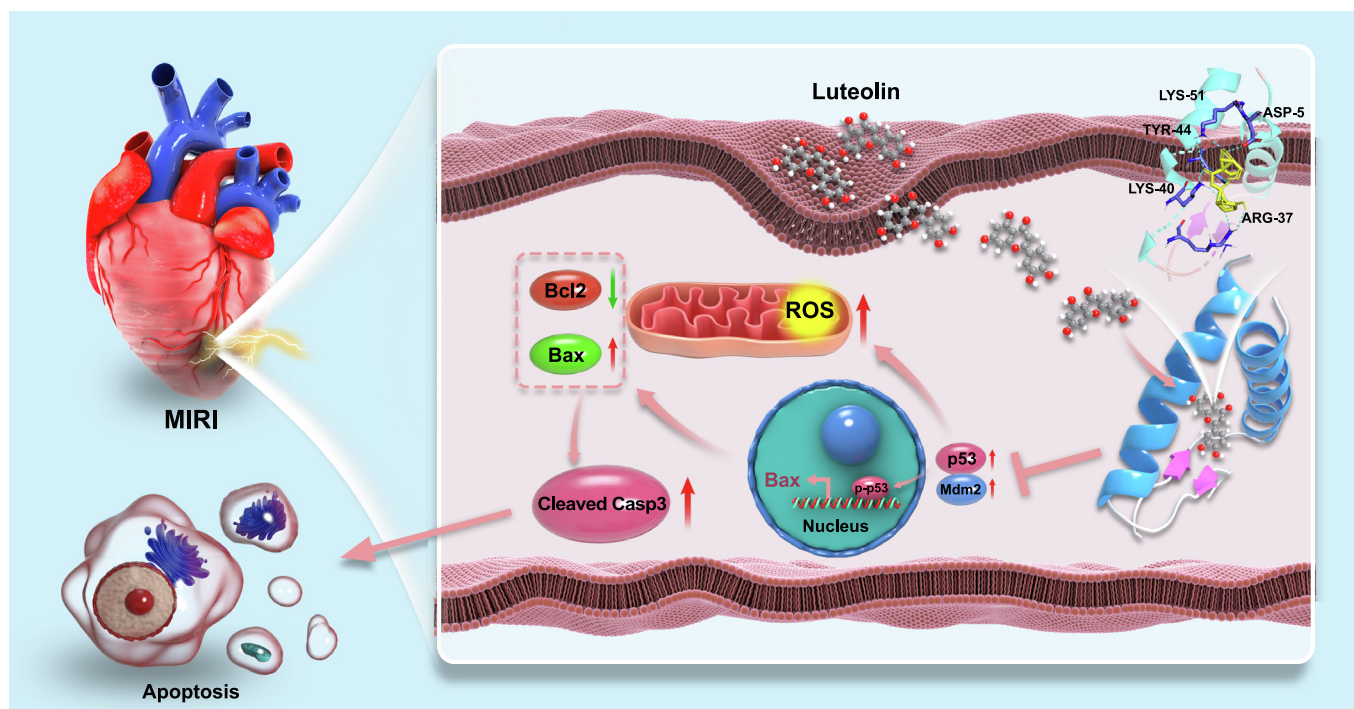


**Fig. 7.** Luteolin suppresses the production of pro-apoptotic proteins and decreases the generation of mitochondrial ROS by inhibiting the accumulation and phosphorylation of p53, consequently mitigating MIRI. Bax: BCL2-associated X protein; Bcl2: B cell lymphoma 2; Casp3: caspase 3; Mdm2: murine double minute 2; MIRI: myocardial ischemia/reperfusion injury; ROS: reactive oxygen species.

- management of acute myocardial infarction in patients presenting with ST-segment elevation of the European Society of Cardiology (ESC). *Eur Heart J* 2018;39(2):119–77.
- [3] Ibanez B, Heusch G, Ovize M, Van de Werf F. Evolving therapies for myocardial ischemia/reperfusion injury. *J Am Coll Cardiol* 2015;65(14):1454–71.
  - [4] Frohlich GM, Meier P, White SK, Yellon DM, Hausenloy DJ. Myocardial reperfusion injury: looking beyond primary PCI. *Eur Heart J* 2013;34(23):1714–22.
  - [5] Yano T, Abe K, Tanno M, Miki T, Kuno A, Miura T, et al. Does p53 inhibition suppress myocardial ischemia-reperfusion injury? *J Cardiovasc Pharmacol Ther* 2018;23(4):350–7.
  - [6] Imran M, Rauf A, Abu-Izneid T, Nadeem M, Shariati MA, Khan IA, et al. Luteolin, a flavonoid, as an anticancer agent: a review. *Biomed Pharmacother* 2019;112:108612.
  - [7] Muruganathan N, Dhanapal AR, Baskar V, Muthuramalingam P, Selvaraj D, Aara H, et al. Recent updates on source, biosynthesis, and therapeutic potential of natural flavonoid luteolin: a review. *Metabolites* 2022;12(11):1145.
  - [8] Kim S, Chin YW, Cho J. Protection of cultured cortical neurons by luteolin against oxidative damage through inhibition of apoptosis and induction of heme oxygenase-1. *Biol Pharm Bull* 2017;40(3):256–65.
  - [9] Chang H, Li C, Huo KY, Wang QY, Lu LH, Zhang Q, et al. Luteolin prevents H<sub>2</sub>O<sub>2</sub>-induced apoptosis in H9C2 cells through modulating Akt-P53/Mdm2 signaling pathway. *Biomed Res Int* 2016;2016:5125836.
  - [10] Luo YY, Shang PP, Li DY. Luteolin: a flavonoid that has multiple cardio-protective effects and its molecular mechanisms. *Front Pharmacol* 2017;8:692.
  - [11] Wei B, Lin Q, Ji YG, Zhao YC, Ding LN, Zhou WJ, et al. Luteolin ameliorates rat myocardial ischaemia-reperfusion injury through activation of peroxiredoxin II. *Br J Pharmacol* 2018;175(16):3315–32.
  - [12] Yu DS, Li MW, Tian YQ, Liu J, Shang J. Luteolin inhibits ROS-activated MAPK pathway in myocardial ischemia/reperfusion injury. *Life Sci* 2015;122:15–25.
  - [13] Zhou XR, Ru XC, Xiao C, Pan J, Lou YY, Tang LH, et al. Sestrin2 is involved in the Nrf2-regulated antioxidative signaling pathway in luteolin-induced prevention of the diabetic rat heart from ischemia/reperfusion injury. *Food Funct* 2021;12(8):3562–71.
  - [14] Zhao LL, Zhou Z, Zhu CS, Fu ZH, Yu DS. Luteolin alleviates myocardial ischemia reperfusion injury in rats via Sirt1/NLRP3/NF-κB pathway. *Int Immunopharmacol* 2020;85:106680.
  - [15] Jiang YH, Yang WJ, Ding JM, Ji J, Wu LW, Zheng YY, et al. Luteolin pretreatment attenuates hepatic ischemia-reperfusion injury in mice by inhibiting inflammation, autophagy, and apoptosis via the ERK/PPAR athway. *PPAR Res* 2022;2022:8161946.
  - [16] Wang HT, Yao XQ, Huang KL, Zhang J, Xiao JR, Guo J, et al. Low-dose dexamethasone in combination with luteolin improves myocardial infarction recovery by activating the antioxidant response. *Biomed Pharmacother* 2022;151:113121.
  - [17] Li L, Luo W, Qian YY, Zhu WW, Qian JC, Li JL, et al. Luteolin protects against diabetic cardiomyopathy by inhibiting NF-β-mediated inflammation and activating the Nrf2-mediated antioxidant responses. *Phytomedicine* 2019;59:152774.
  - [18] Pan QY, Liu Y, Ma WR, Kan RS, Zhu H, Li DY. Cardioprotective effects and possible mechanisms of luteolin for myocardial ischemia-reperfusion injury: a systematic review and meta-analysis of preclinical evidence. *Front Cardiovasc Med* 2022;9:685998.
  - [19] Hostettler GL, Ralston RA, Schwartz SJ. Flavones: food sources, bioavailability, metabolism, and bioactivity. *Adv Nutr* 2017;8(3):423–35.
  - [20] Lindsey ML, Bolli R, Carty Jr JM, Du XJ, Frangogiannis NG, Frantz S, et al. Guidelines for experimental models of myocardial ischemia and infarction. *Am J Physiol Heart Circ Physiol* 2018;314(4):H812–38.
  - [21] Kim SH, Chen J, Cheng TJ, Gindulyte A, He J, He SQ, et al. PubChem in 2021: new data content and improved web interfaces. *Nucleic Acids Res* 2021;49(D1):D1388–95.
  - [22] Gfeller D, Grosdidier A, Wirth M, Daina A, Michielin O, Zoete V. SwissTargetPrediction: a web server for target prediction of bioactive small molecules. *Nucleic Acids Res* 2014;42(Web server issue):W32–8.
  - [23] Szklarczyk D, Santos A, von Mering C, Jensen LJ, Bork P, Kuhn M. STITCH 5: augmenting protein-chemical interaction networks with tissue and affinity data. *Nucleic Acids Res* 2016;44(D1):D380–4.
  - [24] Bai LL, Chen H, Zhou P, Yu J. Identification of tumor necrosis factor-α (TNF-α) inhibitor in rheumatoid arthritis using network pharmacology and molecular docking. *Front Pharmacol* 2021;12:690118.
  - [25] Wang YX, Zhang S, Li FC, Zhou Y, Zhang Y, Wang ZW, et al. Therapeutic target database 2020: enriched resource for facilitating research and early development of targeted therapeutics. *Nucleic Acids Res* 2020;48(D1):D1031–41.
  - [26] Wishart DS, Feunang YD, Guo AC, Lo EJ, Marcu A, Grant JR, et al. DrugBank 5.0: a major update to the DrugBank database for 2018. *Nucleic Acids Res* 2018;46(D1):D1074–82.
  - [27] Sun L, Dong SF, Ge YB, Fonseca JP, Robinson ZT, Mysore KS, et al. DiVenn: an interactive and integrated web-based visualization tool for comparing gene lists. *Front Genet* 2019;10:421.
  - [28] Szklarczyk D, Gable AL, Lyon D, Junge A, Wyder S, Huerta-Cepas J, et al. STRING v11: protein-protein association networks with increased coverage, supporting functional discovery in genome-wide experimental datasets. *Nucleic Acids Res* 2019;47(D1):D607–13.
  - [29] Shannon P, Markiel A, Ozier O, Baliga NS, Wang JT, Ramage D, et al. Cytoscape: a software environment for integrated models of biomolecular interaction networks. *Genome Res* 2003;13(11):2498–504.
  - [30] Trott O, Olson AJ. AutoDock Vina: improving the speed and accuracy of docking with a new scoring function, efficient optimization, and multithreading. *J Comput Chem* 2010;31(2):455–61.
  - [31] Pinzi L, Rastelli G. Molecular docking: shifting paradigms in drug discovery. *Int J Mol Sci* 2019;20(18):4331.
  - [32] Ru JL, Li P, Wang JN, Zhou W, Li BH, Huang C, et al. TCMP: a database of systems pharmacology for drug discovery from herbal medicines. *J Cheminform* 2014;6:13.
  - [33] Fang F, Li DY, Pan HJ, Chen D, Qi LL, Zhang RQ, et al. Luteolin inhibits apoptosis and improves cardiomyocyte contractile function through the PI3K/Akt pathway in simulated ischemia/reperfusion. *Pharmacology* 2011;88(3–4):149–58.
  - [34] Wang ZY, Shi W, Wu TB, Peng T, Wang XM, Liu SY, et al. A high-throughput drug screening identifies luteolin as a therapeutic candidate for pathological cardiac hypertrophy and heart failure. *Front Cardiovasc Med* 2023;10:1130635.
  - [35] Neubauer S. The failing heart—an engine out of fuel. *N Engl J Med* 2007;356(11):1140–51.
  - [36] Ramachandra CJA, Hernandez-Resendiz S, Crespo-Avilan GE, Lin YH, Hausenloy DJ. Mitochondria in acute myocardial infarction and cardioprotection. *EBioMedicine* 2020;57:102884.
  - [37] Hernandez-Resendiz S, Prunier F, Girao H, Dorn G, Hausenloy DJ. Targeting mitochondrial fusion and fission proteins for cardioprotection. *J Cell Mol Med* 2020;24(12):6571–85.
  - [38] He ZJ, Li XQ, Wang Z, Cao YQ, Han SX, Li N, et al. Protective effects of luteolin against amyloid beta-induced oxidative stress and mitochondrial impairments through peroxisome proliferator-activated receptor γ-dependent mechanism in Alzheimer's disease. *Redox Biol* 2023;66:102848.
  - [39] Zhang XN, Li MY, Yue Y, Zhang Y, Wu AS. Luteoloside prevents sevoflurane-induced cognitive dysfunction in aged rats via maintaining mitochondrial function and dynamics in hippocampal neurons. *Neuroscience* 2023;516:42–53.
  - [40] Yang Y, Zhang Y, Yang JQ, Zhang MM, Tian T, Jiang Y, et al. Interdependent nuclear co-trafficking of ASPP1 and p53 aggravates cardiac ischemia/reperfusion injury. *Circ Res* 2023;132(2):208–22.
  - [41] Liu H, Pedram A, Kim JK. Oestrogen prevents cardiomyocyte apoptosis by suppressing p38α-mediated activation of p53 and by down-regulating p53 inhibition on p38β. *Cardiovasc Res* 2011;89(1):119–28.
  - [42] Wang XY, Yuan T, Yin NN, Ma XF, Zhang ZB, Zhu Z, et al. Luteoloside protects the uterus from *Staphylococcus aureus*-induced inflammation, apoptosis, and injury. *Inflammation* 2018;41(5):1702–16.
  - [43] Zhang KK, Wang H, Qu D, Chen LJ, Wang LB, Li JH, et al. Luteolin alleviates methamphetamine-induced hepatotoxicity by suppressing the p53 pathway-mediated apoptosis, autophagy, and inflammation in rats. *Front Pharmacol* 2021;12:641917.
  - [44] Kim JW, Shin SK, Kwon EY. Luteolin protects against obese sarcopenia in mice with high-fat diet-induced obesity by ameliorating inflammation and protein degradation in muscles. *Mol Nutr Food Res* 2023;67(6):e2200729.
  - [45] Huang H, Xu JY, Zhang SQ, Zhao J, Liu S, Tian L, et al. A network pharmacology-based approach to explore the active ingredients and molecular mechanism of Shenku Tongmai granules on a rat model with chronic heart failure. *J Pharm Pharmacol* 2023;75(6):764–83.
  - [46] Kang KA, Piao MJ, Hyun YJ, Zhen AX, Cho SJ, Ahn MJ, et al. Luteolin promotes apoptotic cell death via upregulation of Nrf2 expression by DNA demethylase and the interaction of Nrf2 with p53 in human colon cancer cells. *Exp Mol Med* 2019;51(4):1–14.
  - [47] Amin A, Karpowicz PA, Carey TE, Arbiser J, Nahta R, Chen ZG, et al. Evasion of anti-growth signaling: a key step in tumorigenesis and potential target for treatment and prophylaxis by natural compounds. *Semin Cancer Biol* 2015;35(Suppl):S55–77.
  - [48] Chen YH, Zhang XJ, Dantas Machado AC, Ding Y, Chen ZC, Qin PZ, et al. Structure of p53 binding to the BAX response element reveals DNA unwinding and compression to accommodate base-pair insertion. *Nucleic Acids Res* 2013;41(17):8368–76.
  - [49] Wei HD, Qu LZ, Dai SY, Li Y, Wang HL, Feng YL, et al. Structural insight into the molecular mechanism of p53-mediated mitochondrial apoptosis. *Nat Commun* 2021;12(1):2280.
  - [50] Polak Y, Xia Y, Zweier JL, Kinzler KW, Vogelstein B. A model for p53-induced apoptosis. *Nature* 1997;389(6648):300–5.
  - [51] Rivera A, Maxwell SA. The p53-induced gene-6 (proline oxidase) mediates apoptosis through a calcineurin-dependent pathway. *J Biol Chem* 2005;280(32):29346–54.
  - [52] Hussain SP, Amstad P, He P, Robles A, Lupold S, Kaneko I, et al. p53-induced up-regulation of MnSOD and GPx but not catalase increases oxidative stress and apoptosis. *Cancer Res* 2004;64(7):2350–6.
  - [53] Rawat L, Balan M, Sasamoto Y, Sabarwal A, Pal S. A novel combination therapy with cabozantinib and honokiol effectively inhibits c-Met-Nrf2-induced renal tumor growth through increased oxidative stress. *Redox Biol* 2023;68:102945.
  - [54] Yu FF, Yu SY, Sun L, Zuo J, Luo KT, Wang M, et al. T-2 toxin induces mitochondrial dysfunction in chondrocytes via the p53-cyclophilin D pathway. *J Hazard Mater* 2023;465:133090.